American Scientific Research Journal for Engineering, Technology, and Sciences (ASRJETS)
ISSN (Print) 2313-4410, ISSN (Online) 2313-4402

http://asrjetsjournal.org/

Evaluation of S355NL Steel Welded by Flux Cored Arc Welding Using Different Tubular Wires

Camila Fagundes de Paula Guedes[a], Gláucio Soares da Fonseca[b]*, Elivelton Alves Ferreira[c], Lucas Rosate Leite dos Santos[d], Marcio Teodoro Fernandes[e], Leonardo Martins Da Silva[f]

[a-f]Escola de Engenharia Industrial Metalúrgica de Volta Redonda (EEIMVR), Graduate Program on Metallurgical Engineering, Federal Fluminense University, Avenida dos Trabalhadores, 420, Vila Santa Cecília, Volta Redonda, Rio de Janeiro, 27255-125, Brazil. Tel: +55-24-2107-3728

[a]Email: camilafagu4@hotmail.com,[b]Email: glauciofonseca@id.uff.br,[c]Email: eliveltonalves@id.uff.br,[d]Email: lucas_rosate@id.uff.br,[e]Email: teodoro_fernandes@id.uff.br,[f]Email: leonardouffsilva@gmail.com

Abstract

High strength low alloy (HSLA) steels are used in several industrial sectors, as they have good mechanical strength and easy weldability. This HSLA is present in several areas, such as naval, petrochemical, piping, and civil construction. S355 NL steel is HSLA grade and has its application in the manufacture of the Brazilian submarine. For the manufacture and finishing of a Brazilian submarine, countless welds are performed during the assembly steps. The welding process currently applied is FCAW (Flux Cored Arc Welding), and the currently applied filler metal is of French origin. However, this import, from France to Brazil, makes manufacturing costs high and the waiting time for the imported product to arrive is long. Thus, in this work, the idea was to characterize a national filler metal (Brazilian) that similarly maintained the microstructure and consequently its mechanical and electrochemical properties concerning the imported filler metal (French). Therefore, the present work aimed at the microstructural, mechanical, and electrochemical characterization of S355NL structural steel welded by the FCAW process with national tubular wire (Brazilian) and imported tubular wire (French). We performed microstructural characterization with the aid of optical microscopy (OM) and scanning electron microscopy (SEM). For the mechanical characterization, we performed the following tests: tensile test, Vickers hardness, and impact at room temperature and -40ºC. In the electrochemical characterization, it generated polarization curves where the samples were exposed to a 3.5% NaCl solution to test the behavior in corrosive media. The results showed that the wires, national and imported, behaved homogeneously and uniformly concerning the mechanical properties.

---

* Corresponding author.

In the electrochemical part, the national material presented in the weld metal a corrosion current density interesting. Therefore, the national tubular wire is a promising filler metal for the welding application of this Brazilian submarine.

Keywords: S355 NL steel; Welding; Tubular wire; Submarine; Mechanical properties; Electrochemical behavior.

1. Introduction

High strength low alloy (HSLA) steels have emerged to replace carbon steels in the automotive industry [1–3]. Alloying elements are added to carbon steel to change its standard microstructure and, therefore, its mechanical properties. HSLA has better mechanical properties than carbon steel. In general, the HSLA has a ferritic-pearlitic structure [1,4,5]. HSLA is currently used in several industrial fields, such as automotive, oil, and gas [6]. S355 NL steel (N - normalized; L - for low-temperature environments) is one of the HSLA classes [7,8]. S355NL steel has a minimum yield strength of 355 MPa [9] and a maximum ultimate tensile strength limit of 730 MPa [2]. The welding process is usually common in the use of these steels. An important step in the design and fabrication of welded structures is to select the welding process and the filler metal [10]. These two factors control the thermal distribution and the microstructure in the weld zone. S355 steel possesses good weldability. It is possible to weld this steel through countless welding processes [11]. The S355 NL steel of the present study is used in the assembly of a Brazilian submarine. For the manufacture and finishing of a Brazilian submarine, countless welds are performed during the assembly steps. The welding process currently applied is FCAW (Flux Cored Arc Welding), and the currently applied filler metal is of French origin. However, this import, from France to Brazil, makes manufacturing costs high and the waiting time for the imported product to arrive is long. Thus, in this work, the idea was to characterize a national filler metal (Brazilian) that similarly maintained the microstructure and consequently its mechanical and electrochemical properties concerning the imported filler metal (French). Therefore, the present work aimed at the microstructural, mechanical, and electrochemical characterization of S355NL structural steel welded by the FCAW process with national tubular wire (Brazilian) and imported tubular wire (French). Microstructural characterization was performed with the aid of optical microscopy (OM) and scanning electron microscopy (SEM). For the mechanical characterization, the following tests were performed: tensile test, Vickers hardness, and impact at room temperature and -40ºC. In the electrochemical characterization, polarization curves were generated where the samples were exposed to a 3.5% NaCl solution to evaluate the behavior in corrosive media.

2. Materials and Methods

2.1. Materials

The S355NL steel analyzed is of industrial origin. The chemical composition, provided by the manufacturer, is given in Table 1. The manufacturing process was hot rolling. Samples were cut from the plate as received to obtain specimens with dimensions of 200 mm x 450 mm x 10 mm.

Table 1: Chemical composition of S355NL (wt. %)

Element	wt (%)
C	0.151
Si	0.379
Mn	1.570
P	0.012
S	0.001
N	0.003
Cu	0.026
Mo	0.011
Ni	0.036
Cr	0.026
V	0.001
Nb	0.027
Ti	0.002
Al-Ti	0.031
Fe	Bal

We give the mechanical properties provided by the manufacturer in Table 2.

Table 2: Mechanical properties of S355NL

Mechanical properties	
Yield strength (σ_y)	422 MPa
Ultimate Tensile Strength (σ_u)	551 MPa
Elongation (%)	27
Absorbed Energy - - 40°C	≥ 27 J

The filler metals, national (A) and imported (B), are tubular wires according to the classification of the American Welding Society [12]. Flow cored, with a 1.2 mm diameter for both materials. The chemical composition and mechanical properties provided by the national (A) manufacturer are given in Tables 3 and 4.

Table 3: Chemical composition of national (A) tubular wire (wt.%)

Element	wt (%)
C	*
Si	1.000
Mn	0.500
P	0.030
S	0.030
Cu	*
Mo	0.200
Ni	0.500
Cr	0.030
V	0.100
Nb	*
Ti	*
H**	4.00
Fe	Bal

* Not specified; ** Diffusible hydrogen (mL /100 g deposited metal).

Table 4: Mechanical properties of national (A) tubular wire

Mechanical properties	
Yield strength (σ_y)	470 - 600 MPa
Ultimate Tensile Strength (σ_u)	550 – 690 MPa
Elongation (%)	19
Absorbed Energy - - 40°C	27 – 55J

The chemical composition and mechanical properties provided by the international (B) manufacturer are given in Tables 5 and 6.

Table 5: Chemical composition of international (B) tubular wire (wt.%)

Element	wt (%)
C	0.060
Si	0.400
Mn	1.200
P	0.030
S	≤ 0.015
Ni	≤ 0.015
Fe	Bal

Table 6: Mechanical properties of international (B) tubular wire

Mechanical properties	
Yield strength (σ_y)	≥ 460 MPa
Ultimate Tensile Strength (σ_u)	530 – 690 MPa
Elongation (%)	23
Absorbed Energy - - 40°C	≥ 47 J

2.2. Methodology

2.2.1. Welding

The welding process currently applied is FCAW. The arrangement of the type of joint that was used is a top with a V groove, with a bevel angle equal to 25° and a root opening equivalent to 6 mm. The shielding gas, 82% argon, and 18% CO_2, and the gas flow rate was 18 L / min, according to International Standard ISO 14175 [13]. The welding machine used was an Origo Feed 304N P4 ESAB. We carried welding out in the flat position and with reverse polarity. We performed welding with 4 passes. Pass 1 represents the root, and pass 2 is the reinforcement. Passes 3 and 4 are finishing passes. We deposited three mm of the weld at the root, while the reinforcement was 4 mm, and the finishing passes were 3 mm. The heat input used was less than 3.0 KJ/mm (the value showed by an internal company standard). Values close to this heat input are also recommended in

welding stainless steels [14,15].

2.2.2. Macrostructural and Microstructural Characterization

After welding, the specimens were ground with emery paper down to 1200 mesh. The samples were metallographically polished with 1 μm and 0.3 μm Al_2O_3 suspensions. After polishing, the samples were etched either by 8% Nital (macrostructural characterization) or 3% Nital (microstructural characterization). We examined the samples with the aid of an Olympus BX51M optical microscope (OM) coupled to an Olympus SC30 digital camera and a Zeiss scanning electron microscope (SEM), model EVO MA10, which operates with lanthanum hexaboride (LaB6) filaments. The determination of the ferrite mean grain size of the base metal (BM) followed the ASTM E112-10 standard [16]. In the samples, five micrographs of the base metal (BM), heat-affected zone (HAZ), and weld metal (WM) were recorded. A conventional quantitative metallography technique determined the ferrite volume fraction and pearlite volume fraction [17]. The volume fraction is equal to the area fraction.

2.2.3. Mechanical Properties

An Otto Wolpert Werke Tester was used to determine the hardness of the samples. The tests followed the ISO 6507-2:2018 standard [18]. It was possible to get a hardness profile through all regions: base metal (BM), heat-affected zone (HAZ), and weld metal (WM). We carried the tensile tests out according to the ASTM A370 standard [19]. We machined the cylindrical specimens to 6.0 x 30.0 x 10.0 mm. We used the PANTEC 1000 KN testing machine. The speed of the tests was 3.0 mm/min until reaching 5.0% strain, and from this point on, it became 10 mm/min until the rupture of the specimens. We performed the tests with specimens removed in the longitudinal position in the weld center. We performed the Charpy tests according to the BS EN 875: 1995 standard [20]. We machined the specimens to 10.0 x 7.5 x 10.0 mm with a V-notch (2 mm). It carried tests out at room temperature. To test the material in adverse situations, which simulate its application in extreme cases, we performed the test at - 40 °C. A Charpy machine PEN-12 was used. We carried the tests out with 6 specimens, 3 removed from WM, and the other 3 from the HAZ.

2.2.4. Electrochemical Tests

With the aid of Emstat3 + potentiostat together with the PSTrace software, the samples were subjected to the potentiodynamic polarization test. In the execution, an electrochemical cell with an area of 1.1 mm^2 was used, which allowed the evaluation of specific regions of the welded joint, such as HAZ and WM. The reference electrode used was Ag/AgCl, and the counter electrode was platinum (Pt). All measurements were programmed to start after 30 minutes of open-circuit potential (OCP), starting from a potential of -100 mV (vs. OCP). After the OCP, the polarization curve was taken. The scanning speed was 1 mV/s. The initial potential was -0.10 V (vs. OCP), and the final voltage was +0.30 V (vs. OCP). The tests were conducted in a solution containing 3.5% sodium chloride (NaCl) at room temperature. Measured potentiodynamic curves were analyzed using Tafel fit by Origin software. The general polarization curve characteristics (corrosion potential - E_{Corr}, corrosion current density - i_{Corr}) were obtained.

3. Results and Discussion

3.1. Macrostructural Characterization

The evaluation of variations in the weld bead is useful because they indicate the conditions under which the weld pool has been distributed in the weld bead. How this distribution occurs can affect the microstructure of the weld pool, also affecting the hardness. Figure 1 shows the sample A macrography (on the left) and sample B macrography (on the right), units in mm.

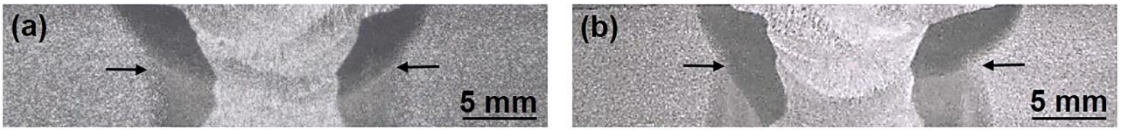

Figure 1: a) Sample A macrography (National), b) Sample B Macrography (imported), units in mm.

For the samples of the Brazilian consumable, figure 1a, and of French origin, figure 1b, it is observed that there was a homogeneous distribution in the weld bead. There is no discontinuity in the welded region.

3.2. Microstructural Characterization

Figure 2 shows the micrographs of the base metal (BM) - S355NL steel.

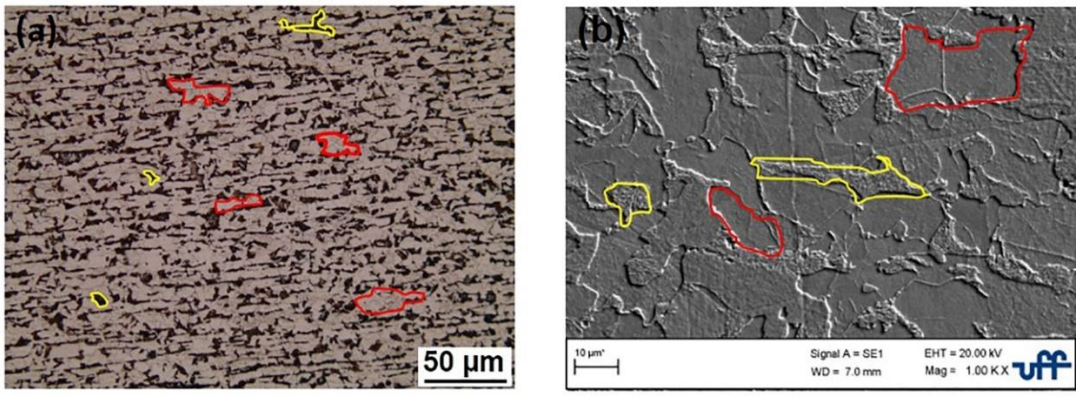

Figure 2: Base metal micrography with ferritic grains (highlighted in red), and pearlite (highlighted in yellow). a) Optical microscopy and b) Scanning electron microscopy

The microstructure of S355NL steel is formed by ferrite-pearlite (figure 2), which is commonly found in the literature [5,8]. The ferritic grain size was 10.0 ± 2.0 µm. In the work of Borko and coauthors [5,8], they also found this value in BM, the ferrite volume fraction was 73.7 ± 1.1%, and the pearlite volume fraction was 26.3 ± 0.9%.

Figure 3 shows the HAZ microstructure in sample A and sample B.

Figures 3a and 3b show acicular ferrite and pearlite. Visually, the morphology of the HAZ is similar between

samples A and B. Acicular ferrite-dominated microstructure is one of the most attractive candidate microstructure because of its high tensile strength, excellent impact toughness, and good weldability [21–23]. Some recognize that the multi-phase microstructure with "soft" ferrite/pearlite "hard" or acicular ferrite/martensite can achieve a wonderful combination of mechanical properties.

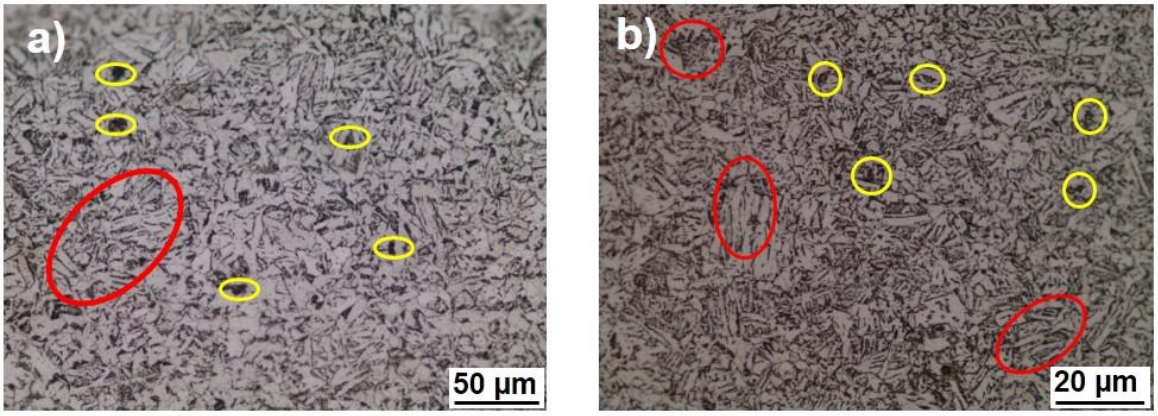

Figure 3: a) HAZ Microstructure of sample A and b) HAZ Microstructure of sample B. Highlighting in red - acicular ferrite grains (light brown). Highlighting in yellow–pearlite (black).

The microstructure of the HAZ shown in Figures 3a and 3b is more refined compared to the microstructure of the base metal (Figure 2a), but the volume fractions of ferrite and pearlite in the HAZ are practically the same as that presented in the BM. For the HAZ of sample A (Figure 3a), the volume fraction of ferrite was 75.0 ± 1.2%, and the volume fraction of pearlite was 25.3% ± 1.3%. For the HAZ of sample B (Figure 3b), the volume fraction of ferrite was 77.2 ± 1.5%, and the volume fraction of pearlite was 22.8% ± 1.8%. Figure 4 shows the microstructure of the WM in samples A and B. In the weld metal of samples A and B, unlike the HAZ, Figures 3a and 3b, the morphologies presented are different. In the weld metal of sample A, the ferrite is closer to the equiaxial morphology (Figure 4a). In the weld metal of sample B, ferrite is acicular and as Widmanstätten (Figure 4b). For the WM of sample A (Figure 4a), the ferrite volume fraction was 88.2 ± 0.5%, and the pearlite volume fraction was 11.8% ± 1.0%. For the WM of sample B (Figure 4b), the ferrite volume fraction was 87.6 ± 1.3%, and the pearlite volume fraction was 12.4% ± 2.0%. One can see that there is a greater amount of ferrite in the WM, figure 4, compared to BM and HAZ, Figures 2 and 3, respectively. This result shows that the cooling in the weld pool was sufficient for the appearance and growth of the ferrite, forming recovered/recrystallized ferrite grains in sample A and acicular ferrite and Widmanstätten in sample B. The morphology of the microstructure shown in sample 4b is like that found by Borko and coauthors [5,8] in the weld metal.

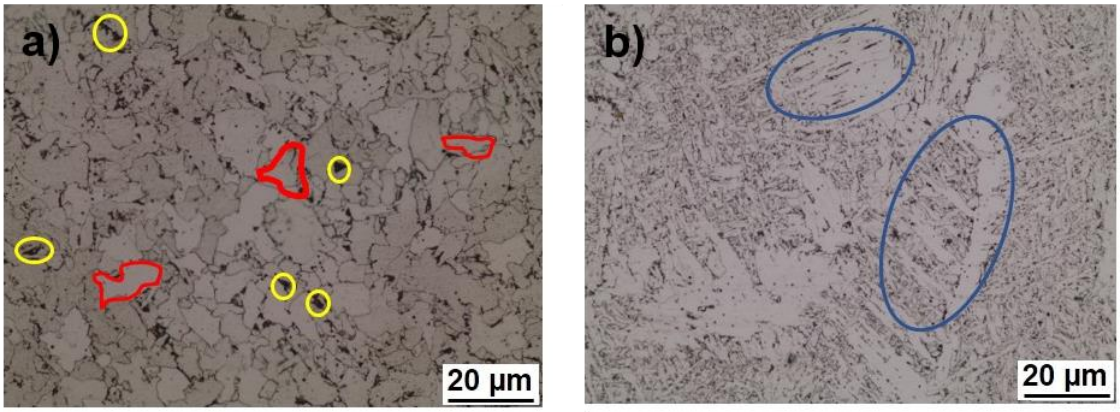

Figure 4: a) WM Microstructure of sample A. Highlighting in red - ferrite grains equiaxed (light brown). Highlighting in yellow - pearlite (black). b) WM Microstructure of sample B. Acicular ferrite (light brown), Widmanstätten ferrite (highlighting in blue), and pearlite (black).

3.3. Mechanical Properties

3.3.1. Hardness Tests

Figures 5 and 6 display the hardness profile performed in the BM, WM, and HAZ for samples A and B, respectively.

Figure 5 shows the results of the sample A hardness tests. One can see the values from 170 to 220 HV with some points on the bottom face, above 200 HV. It is interesting that the hardness values in the WM, measured on the top, bottom, and ½ of the thickness, have values close to that of the BM. Despite the difference in ferrite volume fraction in BM (73.7%) and ferrite volume fraction in WM (88.2%), the hardness values are approximately equal in the regions (BM, WM). Therefore, the morphology of the grains must be taken into account. In BM, Figure 2a, the ferrite has an acicular shape, and in WM, the ferrite has an equiaxial shape, Figure 4a, due to recovery/recrystallization. Recovery/recrystallization, which is common knowledge, reduces crystalline defects. Thus, there was a decrease in the hardness value in WM to values comparable to BM. The highest hardness values, as expected, are at HAZ due to the refinement of the microstructure (Figure 3a). Figure 6 shows that the hardness values for sample B are in a slightly larger range compared to sample A (Figure 5), from 170 to 245 HV. The top side has some points greater than 200 HV in the HAZ region. As explained in the previous paragraph, the structure is more refined in the HAZ, Figure 3b. Soon, the hardness is greater in this region. In WM, Figure 6, as in sample A, Figure 5, there is a decrease in hardness compared to HAZ. However, the values do not return to values compatible with the BM (Figure 5). This may be explained by the morphology found in the WM in sample B. Acicular ferrite grains and Widmanstätten ferrite, Figure 4b. As already found by other authors[15], Widmanstätten's morphology worsens some properties, such as toughness. Making the microstructure harder and more fragile. The range of hardness values found for the material welded with materials A and B, Figures 5 and 6, is within the range recommended by the literature [2,7].

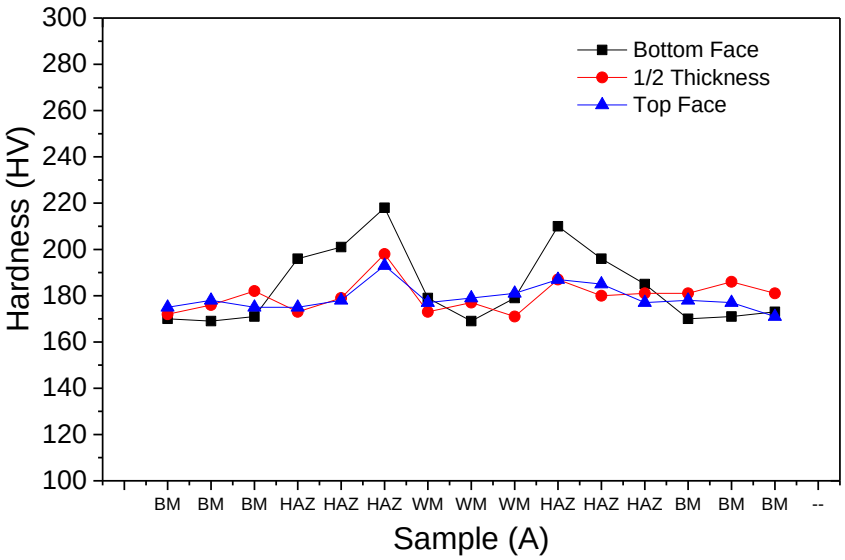

Figure 5: Vickers hardness profile – Sample A. Values measured from the base metal to the base metal, i.e., BM, HAZ, WM, HAZ, BM.

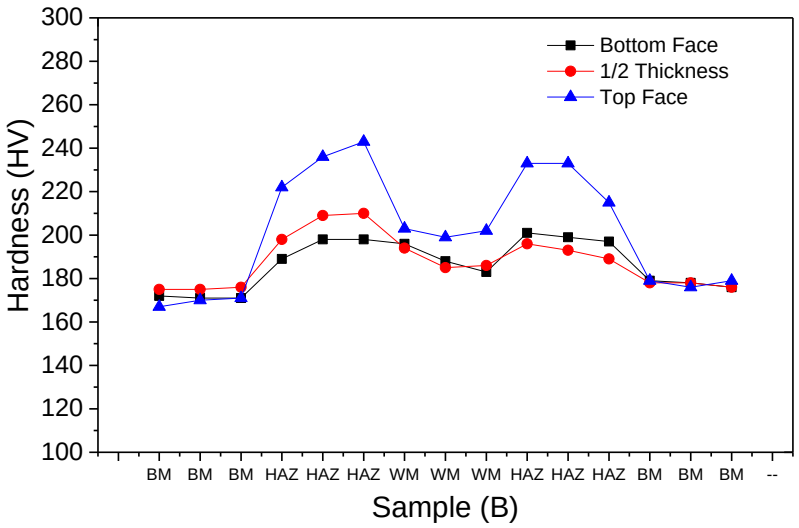

Figure 6: Vickers hardness profile – Sample B. Values measured from the base metal to the base metal, i.e., BM, HAZ, WM, HAZ, BM.

3.3.2. Tensile Tests

Figure 7 shows the stress x strain curves for samples A and B.

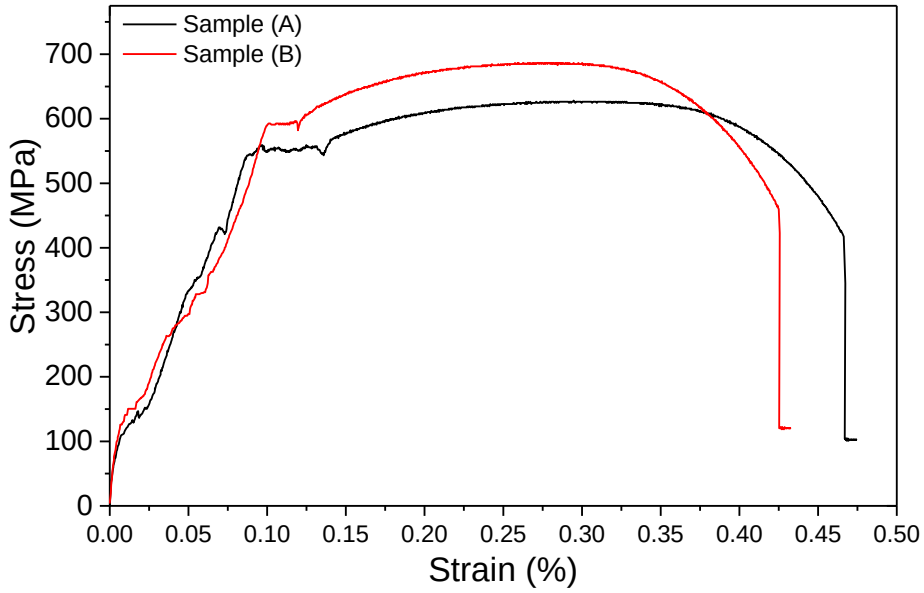

Figure 7: Stress-strain curves of samples A and B.

One can see in Figure 7 that samples A and B had similar behavior. The range value for ultimate tensile strength indicated by wire manufacturer A is between 550-690 MPa (Table 4), and the value found in Figure 7 was approximately 630 MPa. In sample B, in which the manufacturer works in the range of 530-690 MPa for ultimate tensile strength (Table 6), a result of 685 MPa was obtained. Samples A and B are in accordance with the requirements for mechanical properties given in Tables 4 and 6. Applying the traditional Hollomon equation to the data in Figure 7, we find the strength coefficient, K, and the strain hardening exponent, n. Table 7 summarizes the values obtained.

Table 7: Values of strength coefficient, K, and strain hardening exponent, n, for samples A and B.

Sample	K (MPa)	n
A	790	0.16
B	893	0.18

3.3.3. Charpy Impact Test

Figures 8 and 9 show the energy absorbed values by samples A and B in WM and HAZ. The tests were carried out at room temperature and -40 °C.

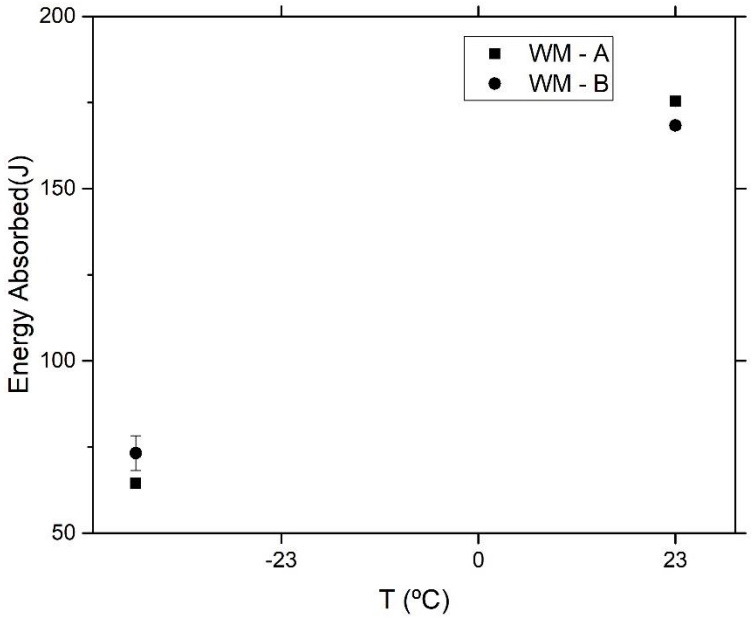

Figure 8: Energy absorbed by samples A and B in WM. Tests were performed at 23ºC and -40°C. The errors measured in some samples are smaller than the symbol used in Figure 8 and are not shown.

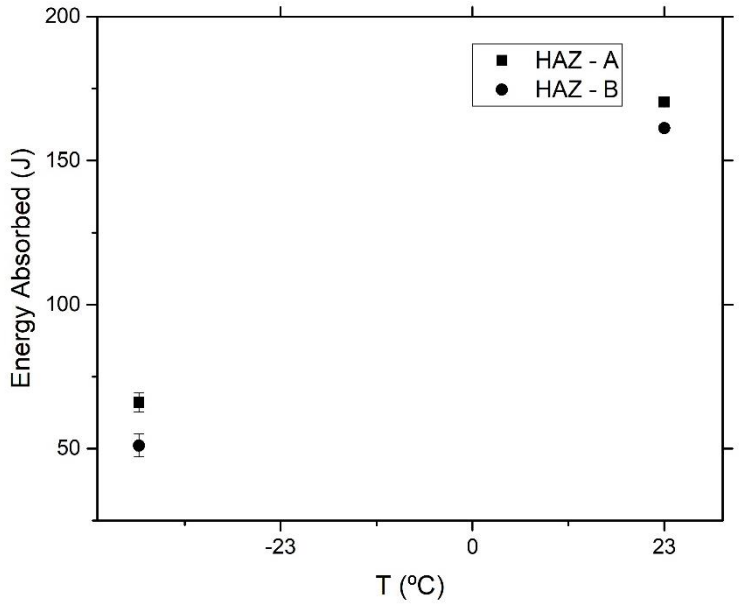

Figure 9: Energy absorbed by samples A and B in HAZ. Tests were performed at 23ºC and -40°C. The errors measured in some samples are smaller than the symbol used in Figure 9 and are not shown.

Figure 8 shows that at room temperature, samples A and B absorb high energy in WM. As the temperature decreases, the energy absorbed in the WM falls. What was to be expected because of the already known ductile-brittle transition temperature in BCC materials [15]. Despite this, the values found for the energy absorbed at -40ºC are under the values provided by the manufacturers presented in Tables 4 and 6. It is also interesting to note that the different ferrite morphologies present in WM, equiaxial, WM-A, Figure 4a, or acicular and

Widmanstätten in WM-B, Figure 4b, have little influence on the energy absorbed by the samples, Figure 8. Based on the results got, the Widmanstätten morphology shows that it has a greater influence on the hardness value (Figures 5 and 6) compared to the absorbed energy (Figure 8). The behavior of the samples concerning the energy absorbed in the HAZ, Figure 9, is like that found in Figure 8 for WM. At room temperature, the samples absorb high energy. With decreasing temperature, the samples absorb less energy. With similar microstructures in the HAZ, Figures 3a and 3b and volumetric fractions of the phases are also similar, the absorbed energies, Figure 9, are also similar. Bearing in mind that the values found for the energy absorbed at -40ºC follow the values provided by the manufacturers presented in Tables 4 and 6.

3.4. Electrochemical Tests

Figure 10 shows the potentiodynamic curves of the BM, HAZ-A, HAZ-B, WM-A, WM-B. After the method of extrapolation of the Tafel curves, it is possible to get the corrosion current densities, i_{corr}. The polarization curves present a typical profile of active material, which does not undergo passivation, that is, a material that suffers generalized corrosion, that is when the material is attacked uniformly on the surface. The lower i_{corr} value shows that the material is more resistant to generalized corrosion.

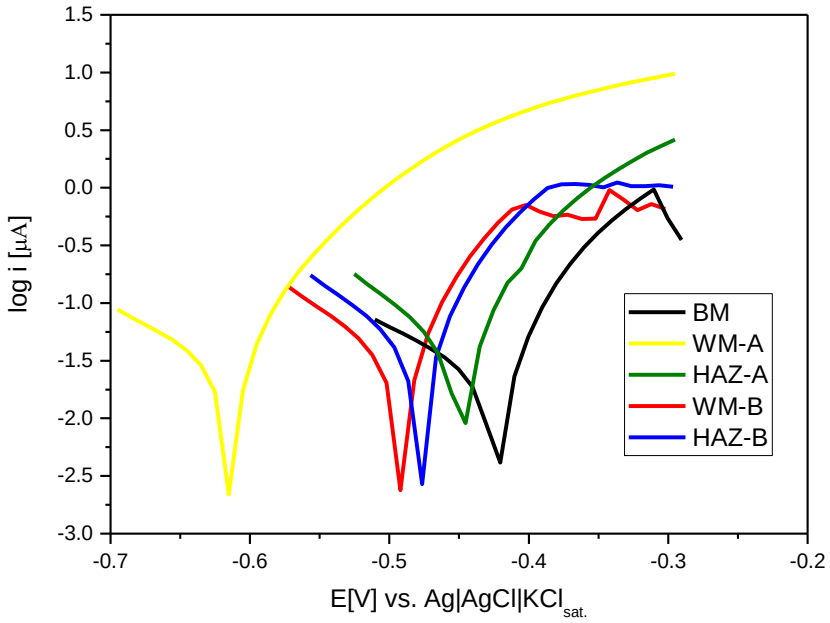

Figure 10: Potentiodynamic curves of BM, HAZ -A, HAZ -B, WM - A, WM - B.

Table 8 shows the electrochemical characteristics for the base metal and the weld regions got from Tafel analysis of the potentiodynamic curves (Figure 10). The area was 1.1 mm^2.

Table 8: Electrochemical characteristics from potentiodynamic curves for the base material and the weld regions.

Region	i_{corr} (μA/cm^2)	E_{corr} (V)
BM	1.86	-0.42
HAZ - A	3.46	-0.45
WM - A	2.39	-0.61
HAZ - B	2.94	-0.48
WM - B	2.62	-0.49

Analyzing figure 10 and table 8, the corrosion current density varied for different regions and got the following corrosion resistance: BM> WM - A> WM - B> HAZ - B> HAZ - A. This result got in this work is interesting. The base metal is more corrosion resistant and follows in the literature. Borko and coauthors [8], working with S355J2 steel, found that the base metal was more resistant than the weld region (WM +HAZ). However, the authors [8] analyzed the weld region as a whole. Did not analyze separately, as performed in this work. In this paper, concerning the weld zone, WM-A was more resistant to corrosion. One possibility for this behavior, (WM-A more corrosion resistant), would be the greater amount of alloying elements in wire A, such as Cr and Mo, making the weld with material A more resistant to corrosion. In theory, this argument should apply to the weld region (WM and HAZ). That is, to increase the corrosion resistance of the weld region with material A. But when analyzing the values for the corrosion current density in Table 8, HAZ-A has a lower corrosion resistance than HAZ-B. Therefore, the alloying elements did not increase the corrosion resistance of HAZ-A compared to HAZ-B. Another possibility to explain the greater resistance to corrosion in WM-A is the type of morphology found in WM. Equiaxial ferrite in WM-A, Figure 4a, and acicular and widmanstätten ferrite in WM-B, Figure 4b. Huang and co-authors [24] pointed out that the ratio of acicular ferrite and Widmanstätten ferrite affects the corrosion rate of welded carbon steel. Thus, the results presented in the electrochemical tests, Figure 10, and Table 8, show that the equiaxial morphology of ferrite can interest in terms of the corrosion resistance of this steel.

4. Conclusions

The work analyzed the welding of S355NL steel by FCAW using 2 different wires as filler metals. One national (Brazilian - A), another imported (French - B). The main conclusions were as follows:

- In the comparison between the weld regions, HAZ - A / HAZ - B and WM - A / WM - B, the percentages of ferrite and pearlite in the material welded with national and imported wire are practically equal. HAZ-A and HAZ-B have a more refined microstructure compared to the base metal. In WM-A, the ferrite morphology is equiaxial. In WM-B, the ferrite morphology is acicular and Widmanstätten;
- The highest hardness values, as was to be expected, were in the HAZ, both for material A and material B, due to the refinement of the microstructure. Despite the difference in ferrite volume fraction in BM (73.7%) and ferrite volume fraction in WM-A (88.2%), the hardness values were approximately equal in the regions (BM, WM-A). Therefore, the morphology of the grains must be taken into account. In BM, ferrite has an acicular form, and in WM-A, ferrite has an equiaxial form due to

recovery/recrystallization. In the recovery/recrystallization process, there is a decrease in crystalline defects, and thus, the hardness values in WM-A have values comparable to those of BM. WM-B has ferrite in the Widmanstätten morphology, so the hardness values are higher when compared to BM;

- The values of yield strength, ultimate tensile strength, and energy absorbed at room temperature and low temperature between samples are similar. The values obtained are within the manufacturers' specification;
- Potentiodynamic tests indicated that the corrosion current density varied between regions. BM is more resistant. Concerning the weld zone, WM-A was more corrosion resistant. This result is probably linked to the equiaxial ferrite obtained in WM-A;
- In general, the results indicated that the wires, national and imported, behaved homogeneously and uniformly concerning the mechanical properties. In the electrochemical part, the national material presented in the weld metal (WM-A), a corrosion current density interesting. Thus, we conclude that the national wire is a promising filler metal for the welding application of this Brazilian submarine.

Acknowledgments

This research was funded by Fundação de Amparo à Pesquisa do Estado do Rio de Janeiro (FAPERJ); The "Conselho Nacional de Desenvolvimento Científico e Tecnológico" (CNPq) is acknowledged for the PQ2 research grant 311996/2018-3 (G.S. Fonseca) This study was financed in part by the Coordenação de Aperfeiçoamento de Pessoal de Nível Superior - Brasil (CAPES) - Finance Code 001.

References

[1]. F. Pastorek, K. Borko, S. Fintová, D. Kajánek, and B. Hadzima, "Effect of Surface Pretreatment on Quality and Electrochemical Corrosion Properties of Manganese Phosphate on S355J2 HSLA Steel," Coatings, vol. 6, no. 4, p. 46, 2016.

[2]. C. I. Garcia, High strength low alloyed (HSLA) steels. Elsevier Ltd, 2016.

[3]. S. R. Nathan, V. Balasubramanian, S. Malarvizhi, and A.G. Rao, and, "Effect of Welding Process on Mechanical and Microstructural Characteristics of High Strength Low Alloy Naval Grade Steel Joints," Defence Technology, vol. 11, no. 3, p. 308-317, 2015.

[4]. V. D. Poznyakov, S.L. Zhdanov, and A. A. Maksimenko, "Structure and properties of welded joints of steel S390 (S355J2)," The Paton Welding Journal, no. 8, pp. 06–10, 2012.

[5]. K. Borko, F. Pastorek, M. N. Jacková, and B. Hadzima, "Electrochemical properties of welded S355J2 steel before and after surface treatment by manganese phosphating," Mater. Today Proc., vol. 5, no. 13, pp. 26482–26488, 2018.

[6]. K. Sirin, S. Y. Sirin, and E. Kaluc, "Influence of the interpass temperature on t8/5 and the mechanical properties of submerged arc welded pipe," J. Mater. Process. Technol., vol. 238, pp. 152–159, 2016.

[7]. L. Kolarik, M. Kolarikova, P. Vondrous, and R. Hrabina, "The choice of parameters for welding of steel S355NL," 23rd DAAAM Int. Symp. Intell. Manuf. Autom. 2012, vol. 2, no. February 2016, pp. 1027–1030, 2012.

[8]. K. Borko, B. Hadzima, and F. Pastorek, "The corrosion properties of S355J2 steel welded joint in

chlorides environment," Period. Polytech. Transp. Eng., vol. 47, no. 4, pp. 342–347, 2019.

[9]. British Standards, "Hot rolled products of structural steels—Part 1: General technical delivery conditions," BS EN 10025-12004, vol. 3, p. 36, 2004.

[10]. H. Alipooramirabad, A. Paradowska, R. Ghomashchi, and M. Reid, "Investigating the effects of welding process on residual stresses, microstructure and mechanical properties in HSLA steel welds," J. Manuf. Process., vol. 28, pp. 70–81, 2017.

[11]. M. Vural, Welding Processes and Technologies, vol. 6. Elsevier, 2014.

[12]. American Welding Society, "Specification for Carbon Steel Electrodes for Flux Cored Arc Welding.," Am. Natl. Stand. Institute, Stand., 2010.

[13]. International Standard ISO 14175, "Welding consumables — Gases and gas mixtures for fusion welding and allied processes," 2008.

[14]. G. R. Mohammed, M. Ishak, S. N. Aqida, and H. A. Abdulhadi, "Effects of heat input on microstructure, corrosion and mechanical characteristics of welded austenitic and duplex stainless steels: A review," Metals (Basel)., vol. 7, no. 2, 2017.

[15]. G. S. Da Fonseca, L. O. R. Barbosa, E. A. Ferreira, C. R. Xavier, and J. A. De Castro, "Microstructural, mechanical, and electrochemical analysis of duplex and superduplex stainless steels welded with the autogenous TIG process using different Heat Input," Metals (Basel)., vol. 7, no. 12, 2017.

[16]. ASTM E112-10, "ASTM International, E112: Standard Test Methods for Determining Average Grain Size," ASTM Int., vol. 96, no. 2004, pp. 1–26, 2004.

[17]. R. Russ, J.C; Dehoff, Practical Stereology, 2nd ed., New York, NY, USA: Kluwer Academic/Plenum Publishers, 2000, pp. 45–78.

[18]. International Standard ISO 6507-2, "Metallic materials — Vickers hardness test - Part 2: Verification and calibration of testing machines," 2018.

[19]. ASTM, "A370: Standard Test Methods and Definitions for Mechanical Testing of Steel Products," ASTM Int., pp. 1–50, 2014.

[20]. British Standards, "Destructive tests on welds in metallic materials — Impact tests — Test specimen location, notch orientation and examination," BS EN 875, 1995.

[21]. D. Liang Ren, F. ren Xiao, P. Tian, X. Wang, and B. Liao, "Effects of welding wire composition and welding process on the weld metal toughness of submerged arc welded pipeline steel," Int. J. Miner. Metall. Mater., vol. 16, no. 1, pp. 65–70, 2009.

[22]. C. Liu, L. Shi, Y. Liu, C. Li, and H. Li, "Acicular ferrite formation during isothermal holding in HSLA steel," J. Mater. Sci., vol. 51, no. 7, pp. 3555–3563, 2016.

[23]. M. C. Zhao, K. Yang, and Y. Y. Shan, "Comparison on strength and toughness behaviors of microalloyed pipeline steels with acicular ferrite and ultrafine ferrite," Mater. Lett., vol. 57, no. 9–10, pp. 1496–1500, 2003.

[24]. H.H. Huang, W.T. Tsai, and J.T. Lee" The Influences Of Microstructure and Composition On The Electrochemical Behavior Of A516 Steel Weldment," Corros. Sci., vol. 36, no. 6, pp. 1027–1038, 1994.